Supporting Information

Direct in Situ Measurement of Charge Transfer Processes During Photoelectrochemical Water Oxidation on Catalyzed Hematite

Jingjing Qiu,[1] Hamed Hajibabaei,[2] Michael R. Nellist,[1] Forrest A. L. Laskowski,[1] Thomas W. Hamann[2] and Shannon W. Boettcher[1*]

[1]Department of Chemistry and Biochemistry, Materials Science Institute, University of Oregon, Eugene, Oregon 97403

[2]Department of Chemistry, Michigan State University, East Lansing, Michigan 48824

Experimental

Atomic layer deposition (ALD) of the α-Fe_2O_3 electrode. Prior to deposition of Fe_2O_3, ~2 nm Ga_2O_3 as an underlayer was deposited on fluorine-doped tin oxide (FTO)-coated aluminoborosilicate glass substrates (Solaronix, 10 $\Omega \cdot sq^{-1}$). Thin films of Ga_2O_3 and Fe_2O_3 were deposited by ALD (Savannah 100, Cambridge Nanotech Inc.), using the procedure described previously.[1,2] Briefly, the FTO glass was cleaned by 15 min sequential sonication in soap, water, and isopropyl alcohol. The Ga_2O_3 was deposited using tris-(dimethylamido)gallium(III) ($Ga_2(NMe_2)_6$) (Strem Chemicals Inc.) as the Ga precursor and H_2O as the oxidant using a procedure modified from a previous report.[3] The Ga cylinder was heated to 150 °C and pulsed for 0.2 s under exposure mode for 8 s, followed by a 12 s purge. A 0.015 s pulse of H_2O was then introduced under the same exposure-purge time to oxidize the Ga precursor. A growth rate of ~ 1.1 Å Ga_2O_3/cycle was measured by spectroscopic ellipsometry (Horiba Jobin Yvon, Smart-SE) on control Si wafers. The Ga_2O_3 coated FTO substrates were subsequently coated with ~ 30 nm of Fe_2O_3 by alternating pulses of ferrocene as the iron precursor and a combination of water and ozone as the oxidant. The ferrocene cylinder, heated to 70 °C, was pulsed for 20 s and was followed by an oxidation cycle which included 10 sub-cycles of a 0.015 s H_2O pulse followed by a 2 s ozone pulse, where each sub-cycle was separated by a 5 s purge. During all depositions, Fe_2O_3 was also grown on control Si substrates to determine the film thickness through spectroscopic ellipsometry. After the deposition of Fe_2O_3, the films were annealed at 500 °C for 30 min with a heating rate of 17 $°C \cdot min^{-1}$, and were allowed to cool to room temperature over 2 h. Subsequently, the films were sintered in a preheated oven at 800 °C for 4 min and then quenched to room temperature by being removed from the oven.

Photochemical metal-organic deposition (PMOD) of $Ni_{0.8}Fe_{0.2}O_x$ electrocatalyst film. Clean substrates are an important prerequisite to achieve defect- and crack-free films. A typical cleaning procedure of ITO or FTO|α-Fe_2O_3 substrates includes 1) physically wiping the substrate with ProWipe-880 Berkshire cleanroom wipes and acetone (99.5%, Mallinckrodt Chemicals) to remove adhered dust particles and 2) sequentially spin-cleaning the substrates with deionized water, acetone, ethanol (200 proof, Decon Laboratories) and isopropanol (99.9% Fisher

Chemical). The $Ni_{0.8}Fe_{0.2}O_x$ film was deposited on the clean substrates following a previously reported method.[4] Precursors used include iron(III) 2-ethylhexanoate (50% in mineral spirits, Alfa Aesar), and nickel(II) 2-ethylhexanoate (78% in 2-ethylhexanoic acid, Sigma Aldrich). Solutions of metal precursor complexes were prepared by dissolving the appropriate ratio of metal complexes in hexanes to achieve an overall 15% w/w solution. Films of the precursor complexes were prepared by spin coating 200 μL of solution at 3000 rpm for 60 s (Laurell model WS-400BZ-6NPP/LITE). The films were then irradiated under UV light (Novascan PSD Pro Series) for 70 min and annealed at 100 ºC in air for 1 h. Fourier transform infrared (FTIR) spectroscopy (Thermo Scientific, Nicolet 6700) was employed to follow the photochemical decomposition of metal-organic complex thin films on a double-side-polished Si wafer.

Fabrication of dual-working-electrode devices. Two types of DWE devices, ITO|$Ni_{0.8}Fe_{0.2}O_x$|Au and α-Fe_2O_3|$Ni_{0.8}Fe_{0.2}O_x$|Au, were fabricated as follows. An electrical contact was made to the ITO or FTO|α-Fe_2O_3 substrate coated with the $Ni_{0.8}Fe_{0.2}O_x$ film using Ag paint (Ag flakes suspended in methyl iso-butylketone, Ted Pella, Inc.) and Sn-Cu wire. The $Ni_{0.8}Fe_{0.2}O_x$ film was carefully scrapped off with a razor blade at the wire contact. Epoxy (Loctite Hysol 1C) was used to cover the contact and keep it isolated from solution. The substrate was attached onto one end of a 3.5-mm-diameter glass tube with the contact wire threaded inside the tube and out of the other end. A 10-nm-thick Au layer was evaporated (rate = 2 $Å \cdot s^{-1}$) from Au metal in an alumina boat (Kurt Lesker) onto the $Ni_{0.8}Fe_{0.2}O_x$ surface and the surrounding epoxy using vacuum thermal evaporation (Angstrom, Amod). Electrical contact was established to the Au film by connecting a second wire to the epoxy surface using Ag paint. A second layer of epoxy was used to cover the contact so that no Ag or Sn-Cu wire was exposed to the electrolyte. The second wire was wrapped around the glass tube and sealed with hot glue. The geometric area of the active surface in a typical device is ~0.01 cm^2. The structure of a DWE device is shown in Scheme S1. The voltages and current densities of ITO or FTO|α-Fe_2O_3 and the $Ni_{0.8}Fe_{0.2}O_x$ film are controlled and measured *via* WE1 and WE2, respectively. The collected V_{WE2} and J_{WE2} thus provide a measure of the voltage of the catalyst layer (V_{cat}) and current density extracted from the top of the catalyst layer (J_{cat}) under the particular experimental conditions chosen, respectively.

Scheme S1. Schematic structure of a semiconductor photoelectrode with separate contacts to catalyst and semiconductor.

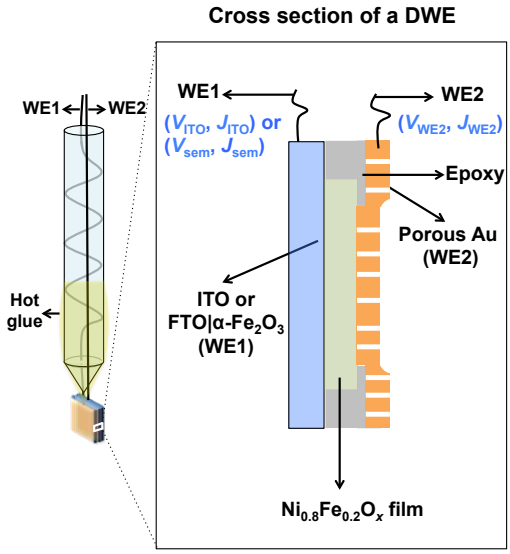

(Photo)electrochemical measurements. Photoelectrochemical measurements were conducted in a three-neck quartz cell containing 20 mL of aq. 0.1 M KOH electrolyte (Fluka Analytical TraceSelect, >30%, diluted with 18.2 MΩ·cm water) using a BioLogic SP-300 potentiostat. A solar simulator (Abet Technologies, model 10500) was used to back-illuminate the photoelectrodes. The intensity was calibrated to ~ 1 sun at the sample surface with a GaP photodiode (Thorlabs), which was used instead of a typical Si photodiode because GaP has a more-similar spectral response to hematite. A Pt coil and a Hg/HgO electrode filled with 1 M KOH (CH instruments) were employed as the counter and the reference electrodes, respectively. The counter-electrode potential sense lead of the BioLogic potentiostat was used to monitor and record the potential of the electrocatalyst when necessary. In separate DWE experiments, for independent control of both contacts, different bipotentiostat channels were used to control/measure WE1 (connected to ITO or FTO|α-Fe_2O_3) and WE2 (the porous Au film in contact with the catalyst). V_{sem} and V_{WE2} represent the voltages of the α-Fe_2O_3 and the porous Au film, respectively, relative to the solution potential $\mathcal{E}_{O_2/OH^-}$ (0.1 M KOH). The OER potential in 1 M KOH is 0.3 V vs. Hg/HgO and V (vs. $\mathcal{E}_{O_2/OH^-}$) = V (vs. Hg/HgO) − 0.359 V is used for conversions in 0.1 M KOH. The electrochemical impedance spectroscopic and photoelectrochemical measurements were made with a Metrohm Autolab potentiostat coupled with Nova electrochemical software. Impedance data were gathered using a 10 mV amplitude perturbation of between 10,000 and 0.01 Hz. Data were fit using NOVA software. It is worth pointing out that the electrodes used in impedance analysis are not DWEs because the Au layer might introduce another interface and cause complication of the data collected.

Materials characterization. Scanning electron microscope (SEM) images were taken using a Zeiss Ultra 55 SEM operating at 5 keV with a 20-μm aperture. Atomic force microscope (AFM) images were collected on a Bruker Dimension Icon using a Tespa v2 probe in tapping

mode. The mass of the $Ni_{0.8}Fe_{0.2}O_x$ film was quantified on a Au/Ti-coated 5 MHz quartz crystal microbalance (QCM) crystal (Stanford Research Systems QCM200). The film mass was calculated based on the Sauerbery equation ($\Delta f = -C_f \times \Delta m$), where Δf is the experimental frequency change, C_f is the sensitivity factor (~ 58 $Hz \cdot cm^2 \cdot \mu g^{-1}$)[5] of the 5 MHz AT-cut quartz crystal in solution, and Δm is the change in mass per area.

Additional figures

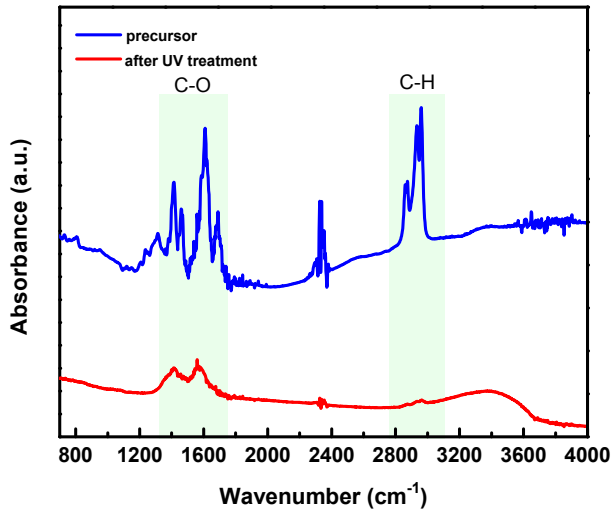

Figure S1. FTIR spectra on the thin films of non-photolyzed precursor film (blue) and the photolyzed film (red). All samples for FTIR were thin films spun-coat on a double-side-polished Si wafer. The green areas indicate the functional groups in the 2-ethylhexanoate ligand.

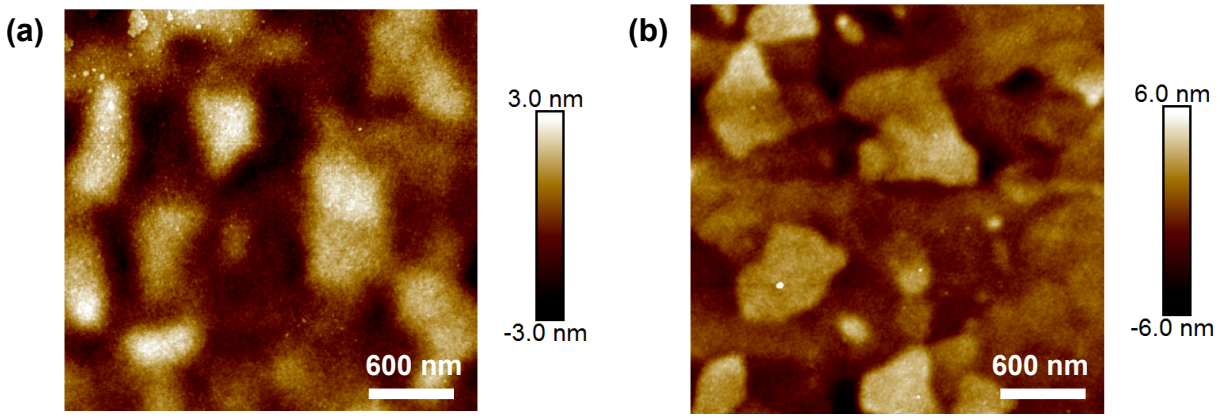

Figure S2. Atomic force microscope (AFM) images of (a) the as-deposited $Ni_{0.8}Fe_{0.2}O_x$ film on an ITO substrate and (b) the $Ni_{0.8}Fe_{0.2}O_x$ film deposited on an ITO substrate after cyclic voltammogram (CV) cycling. The roughening is presumably due to the formation of oxyhydroxide phases under oxygen evolution reaction (OER) conditions in alkaline media.

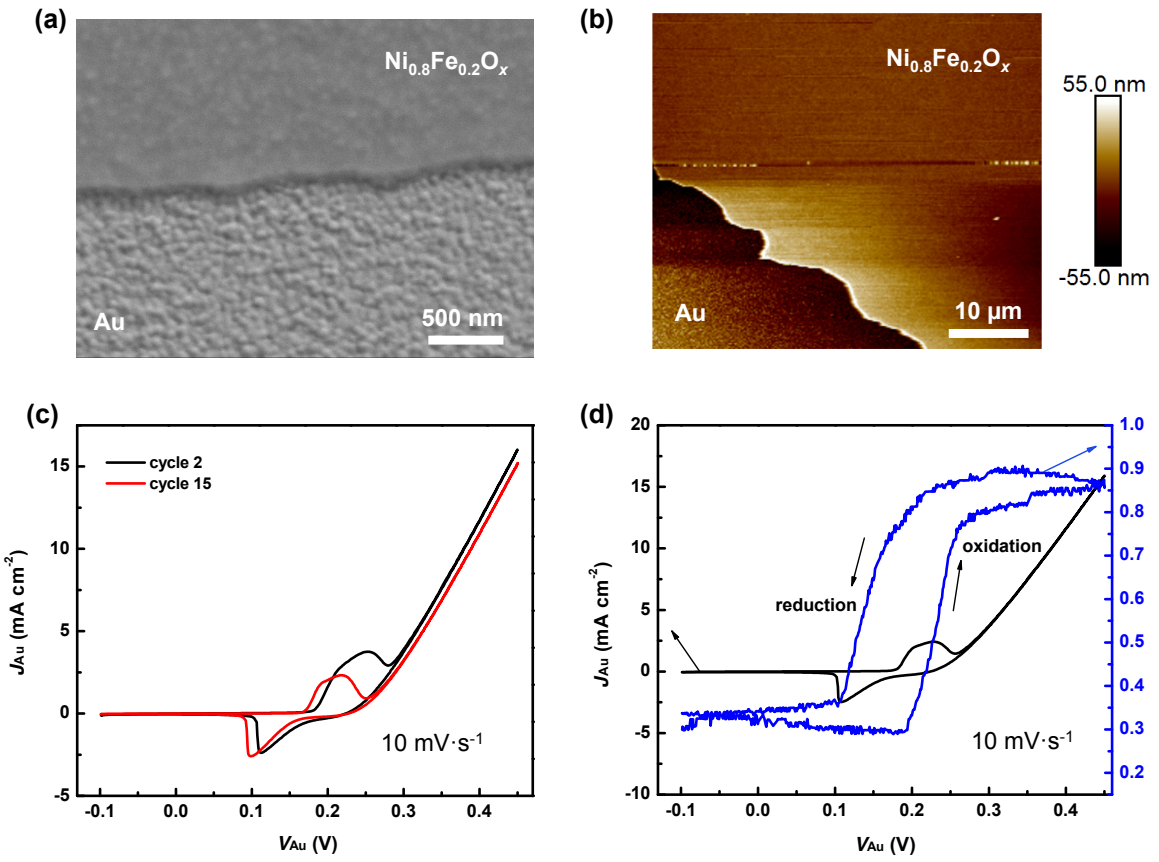

Figure S3. The activation of $Ni_{0.8}Fe_{0.2}O_x$ film on a Au quartz crystal microbalance. (a) Scanning electron microscope (SEM) image of the $Ni_{0.8}Fe_{0.2}O_x$ film on a Au quartz crystal microbalance; (b) AFM image of the $Ni_{0.8}Fe_{0.2}O_x$ film on a Au quartz crystal microbalance; (c) The CVs of the $Ni_{0.8}Fe_{0.2}O_x$ film in 1 M KOH at cycle 2 and cycle 15; (d) The mass change data and corresponding CV from a $Ni_{0.8}Fe_{0.2}O_x$ film in 1 M KOH. The mass of the $Ni_{0.8}Fe_{0.2}O_x$ film (thickness = 65 nm determined from AFM) deposited on the Au quartz crystal microbalance was 12.4 $\mu g \cdot cm^{-2}$, consisting of 1.36×10^{17} Ni atoms. Upon CV cycling, the redox peaks of Ni cathodically shifted and increase in integrated intensity. The mass of the film increases upon oxidation and decreases upon redox. This change in mass during CV cycling is consistent with that previously observed for nominally α-$Ni(OH)_2$.[6] The voltage V_{Au} is the potential applied to the Au QCM, relative to the thermodynamic redox potential for the OER.

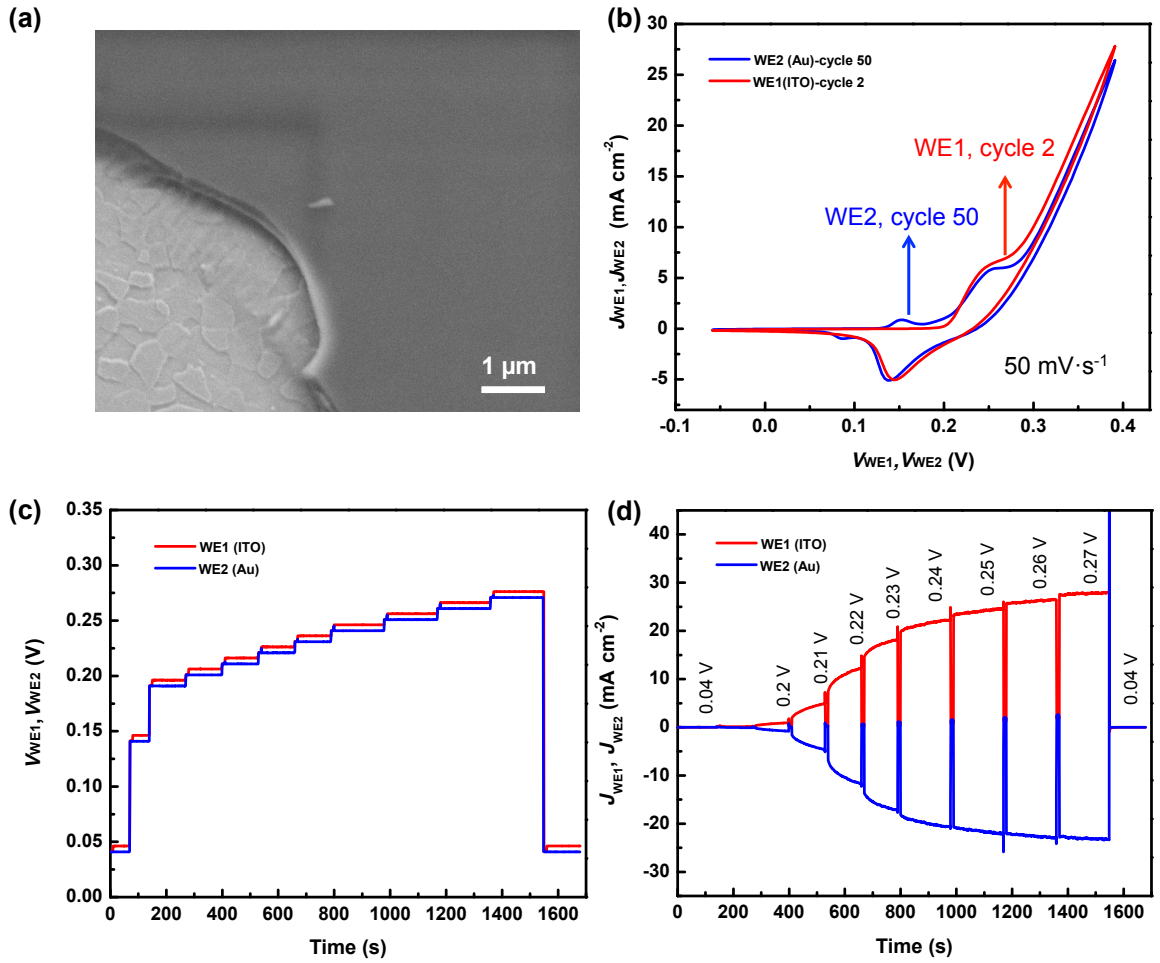

Figure S4. *In situ* measurement of the conductivity of a $Ni_{0.8}Fe_{0.2}O_x$ film using an ITO|$Ni_{0.8}Fe_{0.2}O_x$|Au DWE architecture. (a) SEM image of the $Ni_{0.8}Fe_{0.2}O_x$ film on an ITO substrate. (b) CV curves of $Ni_{0.8}Fe_{0.2}O_x$ from both working electrodes in 0.1 M KOH, respectively. The conditioning of catalyst film was achieved *via* WE2. The CV of catalyst from WE2 at cycle 50 after conditioning and the CV of WE1 at cycle 2 are shown here for comparison. The similarity of the last cycle from WE2 and the initial cycle of WE1 suggests both WE1 and WE2 are fully accessing the film. (c) Time-dependent potential steps of both WEs showing the small voltage offset of 5 mV between WE1 and WE2. (d) Current density measured through the $Ni_{0.8}Fe_{0.2}O_x$ film at WEs 1 and 2 during the voltage steps indicated in (c). The measurement of positive current at WE1 and negative current at WE2 indicates electrons are flowing from WE2 to WE1 through the film and that the magnitude of the current is related to the film conductivity. The voltages V_{WE1} and V_{WE2} are all relative to the thermodynamic redox potential for the OER.

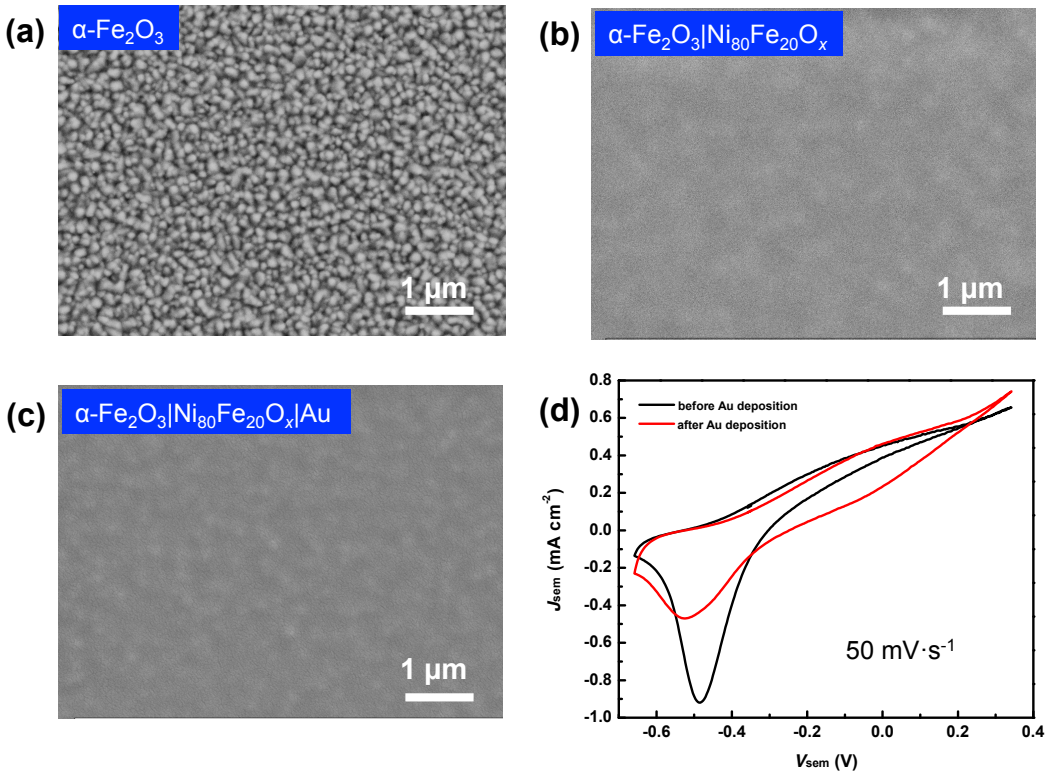

Figure S5. SEM images of (a) α-Fe_2O_3 (b) α-Fe_2O_3|$Ni_{0.8}Fe_{0.2}O_x$ and (c) α-Fe_2O_3|$Ni_{0.8}Fe_{0.2}O_x$|Au. (d) *J*-*V* measurements of α-Fe_2O_3|$Ni_{0.8}Fe_{0.2}O_x$ before and after the coating with of a 10-nm Au film under illumination. The voltage V_{sem} is relative to the thermodynamic redox potential for the OER.

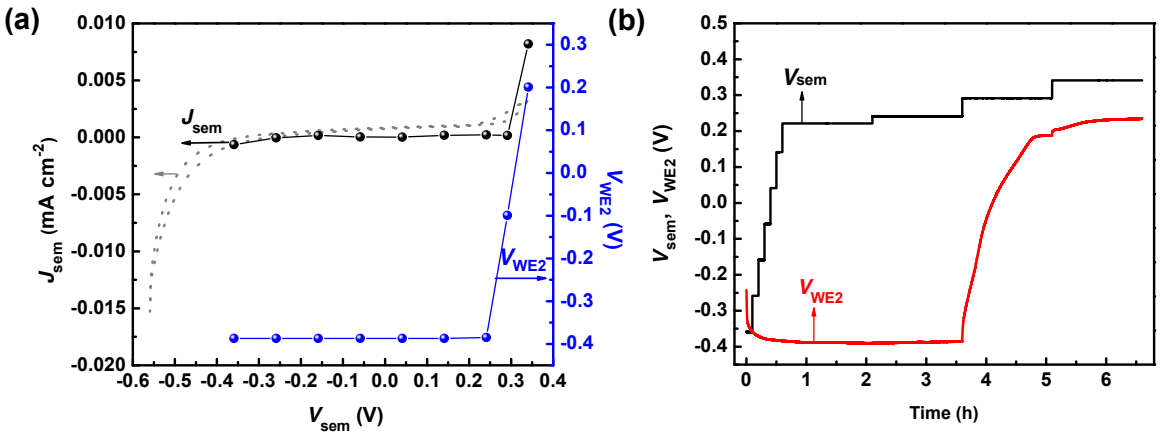

Figure S6. *In situ* measurements of V_{WE2} in response to V_{sem} in the dark. (a) The correlation between V_{WE2} and the steady-state dark current of α-Fe_2O_3. The dashed line represents the CV of α-Fe_2O_3 in the dark (scan rate = 50 mV·s^{-1}). (b) The change of V_{WE2} with V_{sem} over time. The voltages V_{WE2} and V_{sem} are relative to the thermodynamic redox potential for the OER.

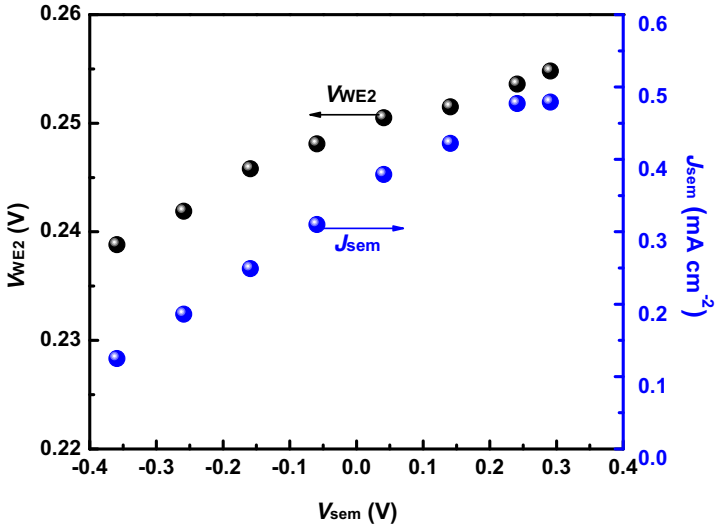

Figure S7. V_{WE2} response on the steady-state current density of illuminated hematite as a function of V_{sem}. The voltages V_{sem} and V_{WE2} are relative to the thermodynamic redox potential for the OER.

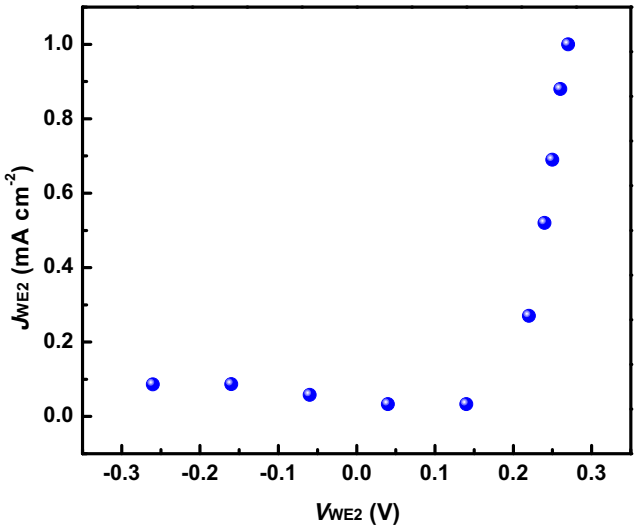

Figure S8. Steady-state current densities of a $Ni_{0.8}Fe_{0.2}O_x$ film under different applied biases vs. $\mathcal{E}_{O_2/OH^-}$ measured from the Au porous film in the dark. The potentials of WE2 ($V_{WE2} = V_{cat}$) were held at different values in a chronoamperometry experiment to record the current densities of the catalyst film ($J_{WE2} = J_{cat}$). We note that for V_{cat} between 0.24 V and 0.26 V, which is the steady-state potential measured under illumination in Fig. S7, the catalyst is passing current similar in magnitude to the photocurrent passed under illumination, consistent with the view that the photogenerated holes move through the catalyst layer. The voltage V_{WE2} is relative to the thermodynamic redox potential for the OER.

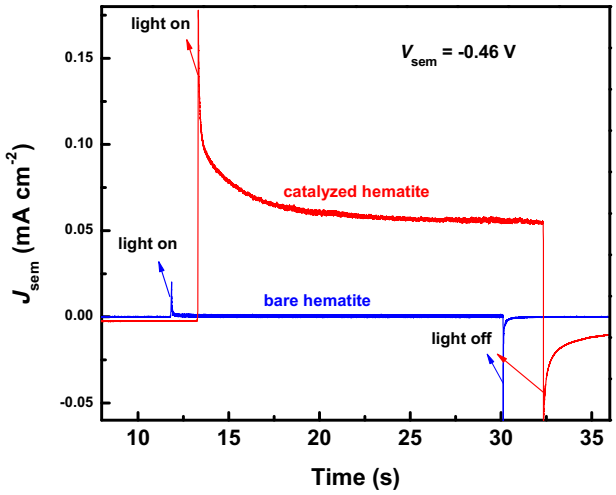

Figure S9. Photocurrent transients of catalyzed and bare hematite electrodes under chopped one-sun illumination. The semiconductor potential V_{sem} is held at -0.46 V vs. $\mathcal{E}_{O_2/OH^-}$. The catalyzed hematite exhibits a peak photocurrent followed by a slow decay to the steady-state Faradaic current. The bare hematite decay is much faster. Both the anodic and cathodic currents of the catalyzed sample are larger than the bare hematite film. These data suggest charge transfer to the catalyst in the case of the catalyzed sample and to surface states in the case of the bare sample. However, knowledge of the portion of surface holes transferred from the semiconductor to the catalyst under operative conditions and what potential the catalyst is sitting at with those holes is impossible to determine with such measurements.

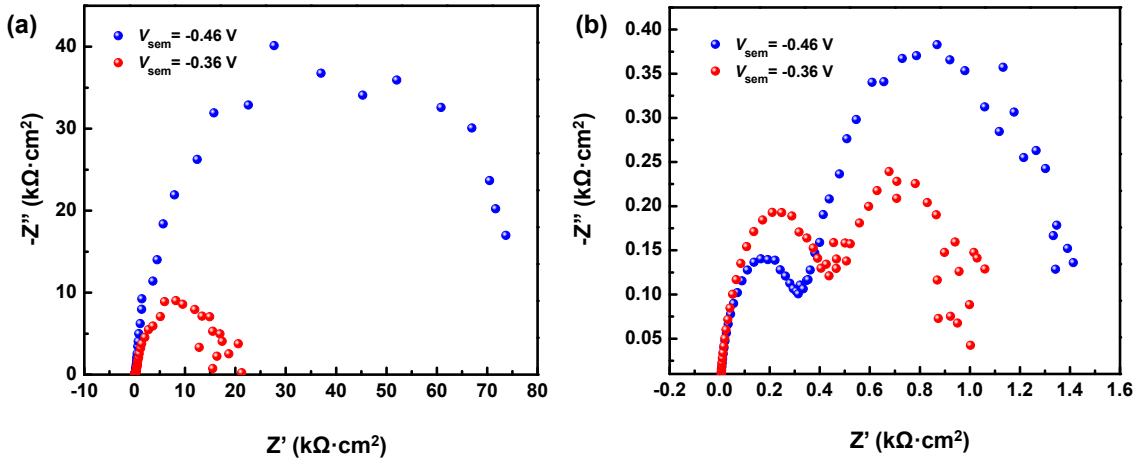

Figure S10. Photoelectrochemical impedance analysis hematite electrodes under one sun illumination. (a) Nyquist plots measured under illumination of a bare hematite electrode; (b) Nyquist plots measured under illumination of a $Ni_{0.8}Fe_{0.2}O_x$ catalyzed hematite electrode. Both

were measured at -0.46 and -0.36 V vs. $\mathcal{E}_{O_2/OH^-}$; potentials near the onset potential for water oxidation under illumination for the catalyst coated electrode. The low frequency semicircle in panel b (right side of the plot) is attributed to capacitance of the catalyst layer and is not present in the electrode without catalyst (panel a). This data is thus consistent with catalyst charging under photoelectrochemical conditions. However, the degree of charging and the efficiency of charge transfer and subsequent water oxidation cannot be determined.

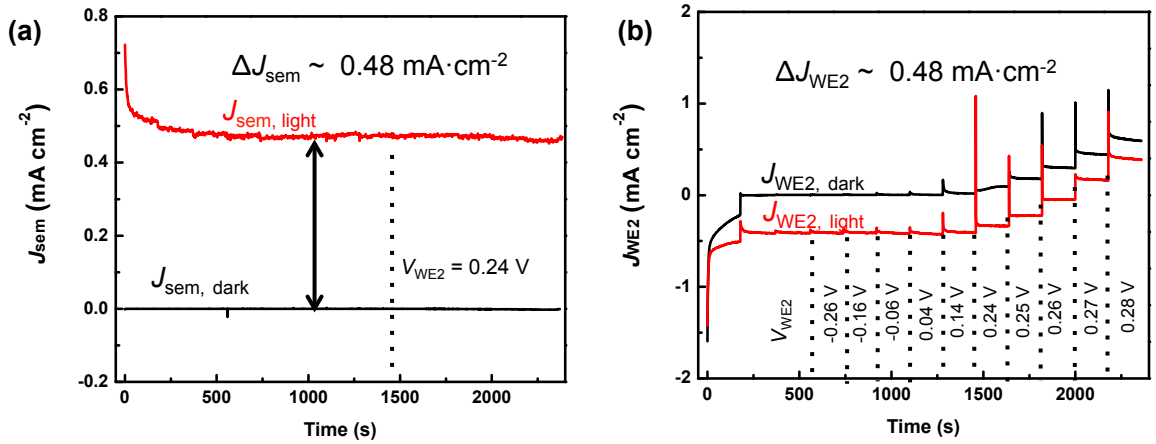

Figure S11. Photogenerated hole transfer at the interface of α-Fe_2O_3|$Ni_{0.8}Fe_{0.2}O_x$. (a) Current densities of α-Fe_2O_3 when V_{sem} is held at 0.1 V vs. $\mathcal{E}_{O_2/OH^-}$ both in the dark (black curve) and under illumination (red curve) while controlling the potentials of the catalyst (V_{WE2} = V_{cat}) in a chronoamperometry experiment. (b) Current densities measured from WE2 under different V_{WE2} vs. $\mathcal{E}_{O_2/OH^-}$ with V_{sem} held at 0.1 V vs. $\mathcal{E}_{O_2/OH^-}$ in the dark (black curve) and under illumination (red curve). Notice that the collection efficiency decreases (i.e. the difference between $J_{WE2,dark}$ and $J_{WE2,light}$ decreases) when V_{WE2} (V_{cat}) is under very anodic biases with V_{sem} held at 0.1 V vs. $\mathcal{E}_{O_2/OH^-}$. The possibility for this decrease is discussed in the main text. The voltages V_{sem} and V_{WE2} are relative to the thermodynamic redox potential for the OER.

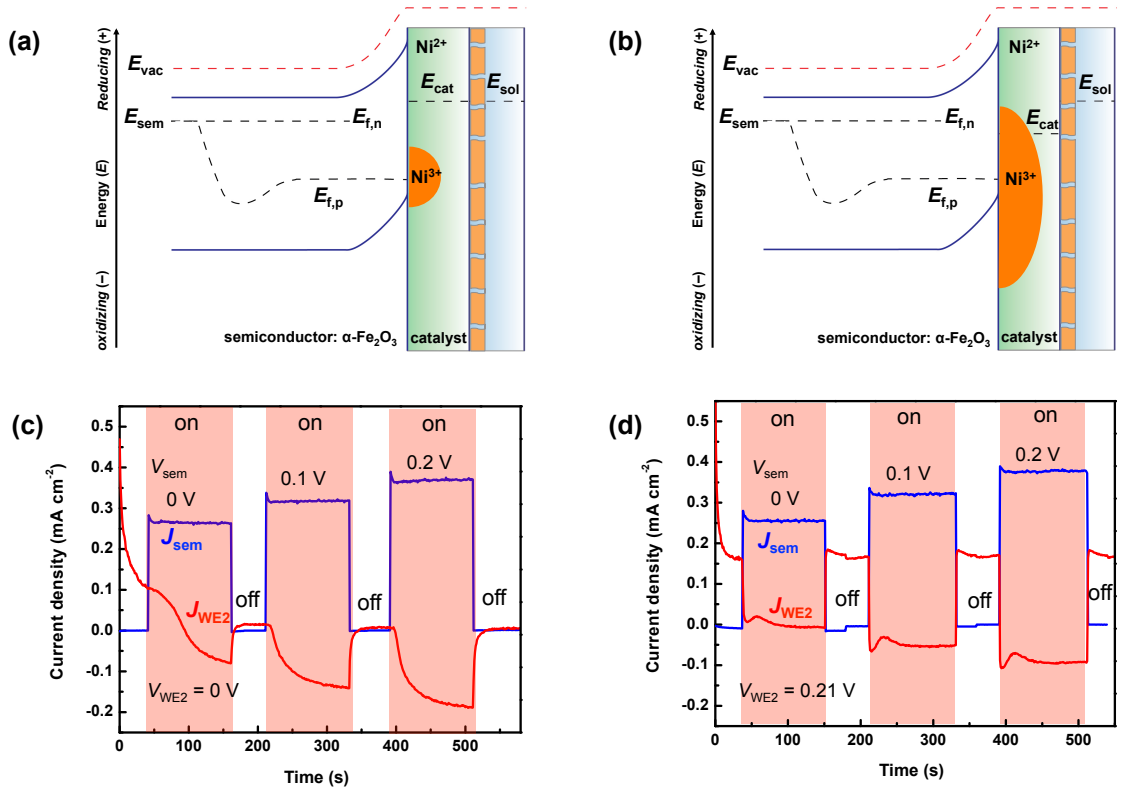

Figure S12. Photogenerated hole transfer at the interface of α-Fe_2O_3|$Ni_{0.8}Fe_{0.2}O_x$. (a) Schematic band structure of the system when V_{WE2} = 0 V vs. $\mathcal{E}_{O_2/OH^-}$; (b) Schematic band structure of the system when V_{WE2} = 0.21 V vs. $\mathcal{E}_{O_2/OH^-}$; (c) *In situ* measurements of J_{WE2} and J_{sem} with V_{WE2} = 0 V vs. $\mathcal{E}_{O_2/OH^-}$ and V_{sem} stepped from 0 V to 0.2 V vs. $\mathcal{E}_{O_2/OH^-}$ under chopped illumination. The catalyst layer is insulating at V_{WE2} (V_{cat}) = 0 V vs. $\mathcal{E}_{O_2/OH^-}$ and therefore the time constant for recording the current at WE2 is slow as a steady-state concentration gradient of holes must be established across the low conductivity catalyst film. (d) *In situ* measurements of J_{WE2} and J_{sem} with V_{WE2} (V_{cat}) = 0.21 V vs. $\mathcal{E}_{O_2/OH^-}$ and V_{sem} stepped from 0 V to 0.2 V vs. $\mathcal{E}_{O_2/OH^-}$ under chopped illumination. When V_{WE2} = 0.21 V vs. $\mathcal{E}_{O_2/OH^-}$, the catalyst layer sits at the onset potential of OER and is conductive. In this scenario, the hole transfer efficiency from hematite to $Ni_{0.8}Fe_{0.2}O_x$ appears higher compared to the case in (a) as the current is easily sensed through WE2 when the catalyst is conductive. Anodic biasing of hematite enhances the hole flux as well as the hole transfer efficiency. This demonstrates that the transfer of photogenerated holes from the semiconductor to the electrocatalyst is kinetically more favorable than water oxidation on the hematite surface under the biasing conditions in this experiment. The voltages V_{sem} and V_{WE2} are relative to the thermodynamic redox potential for the OER.

References:

1. Klahr, B. M.; Martinson, A. B. F.; Hamann, T. W. Photoelectrochemical investigation of ultrathin film iron oxide solar cells prepared by atomic layer deposition. *Langmuir* **2011**, *27*, 461-468.
2. Zandi, O.; Schon, A. R.; Hajibabaei, H.; Hamann, T. W. Enhanced charge separation and collection in high-performance electrodeposited hematite films. *Chem. Mater.* **2016**, *28*, 765-771.
3. Dezelah, C. L.; Niinisto, J.; Arstila, K.; Niinisto, L.; Winter, C. H. Atomic layer deposition of Ga_2O_3 films from a dialkylamido-based precursor. *Chem. Mater.* **2006**, *18*, 471-475.
4. Smith, R. D. L.; Prevot, M. S.; Fagan, R. D.; Zhang, Z. P.; Sedach, P. A.; Siu, M. K. J.; Trudel, S.; Berlinguette, C. P. Photochemical route for accessing amorphous metal oxide materials for water oxidation catalysis. *Science* **2013**, *340*, 60-63.
5. Trotochaud, L.; Young, S. L.; Ranney, J. K.; Boettcher, S. W. Nickel-iron oxyhydroxide oxygen-evolution electrocatalysts: the role of intentional and incidental iron incorporation. *J. Am. Chem. Soc.* **2014**, *136*, 6744-6753.
6. Wehrens-Dijksma, M.; Notten, P. H. L. Electrochemical quartz microbalance characterization of $Ni(OH)_2$-based thin film electrodes. *Electrochim. Acta* **2006**, *51*, 3609-3621.